LA-UR-25-31131
Accepted Manuscript

A new interatomic potential for mixed Mg-Al-Ga-In spinels

Rushton, M.J.D.
Cooper, Michael William Donald
Pilania, Ghanshyam
Uberuaga, Blas P.

Provided by the author(s) and the Los Alamos National Laboratory (1930-01-01).

To be published in: Computational Materials Science

DOI to publisher's version: 10.1016/j.commatsci.2026.114492

Permalink to record:
https://permalink.lanl.gov/object/view?what=info:lanl-repo/lareport/LA-UR-25-31131

Los Alamos National Laboratory, an affirmative action/equal opportunity employer, is operated by Triad National Security, LLC for the National Nuclear Security Administration of U.S. Department of Energy under contract 89233218CNA000001. By approving this article, the publisher recognizes that the U.S. Government retains nonexclusive, royalty-free license to publish or reproduce the published form of this contribution, or to allow others to do so, for U.S. Government purposes. Los Alamos National Laboratory requests that the publisher identify this article as work performed under the auspices of the U.S. Department of Energy. Los Alamos National Laboratory strongly supports academic freedom and a researcher's right to publish; as an institution, however, the Laboratory does not endorse the viewpoint of a publication or guarantee its technical correctness.

Graphical Abstract

A new interatomic potential for mixed Mg-Al-Ga-In spinels

Michael J. D. Rushton, Michael W. D. Cooper, Ghanshyam Pilania, Blas P. Uberuaga

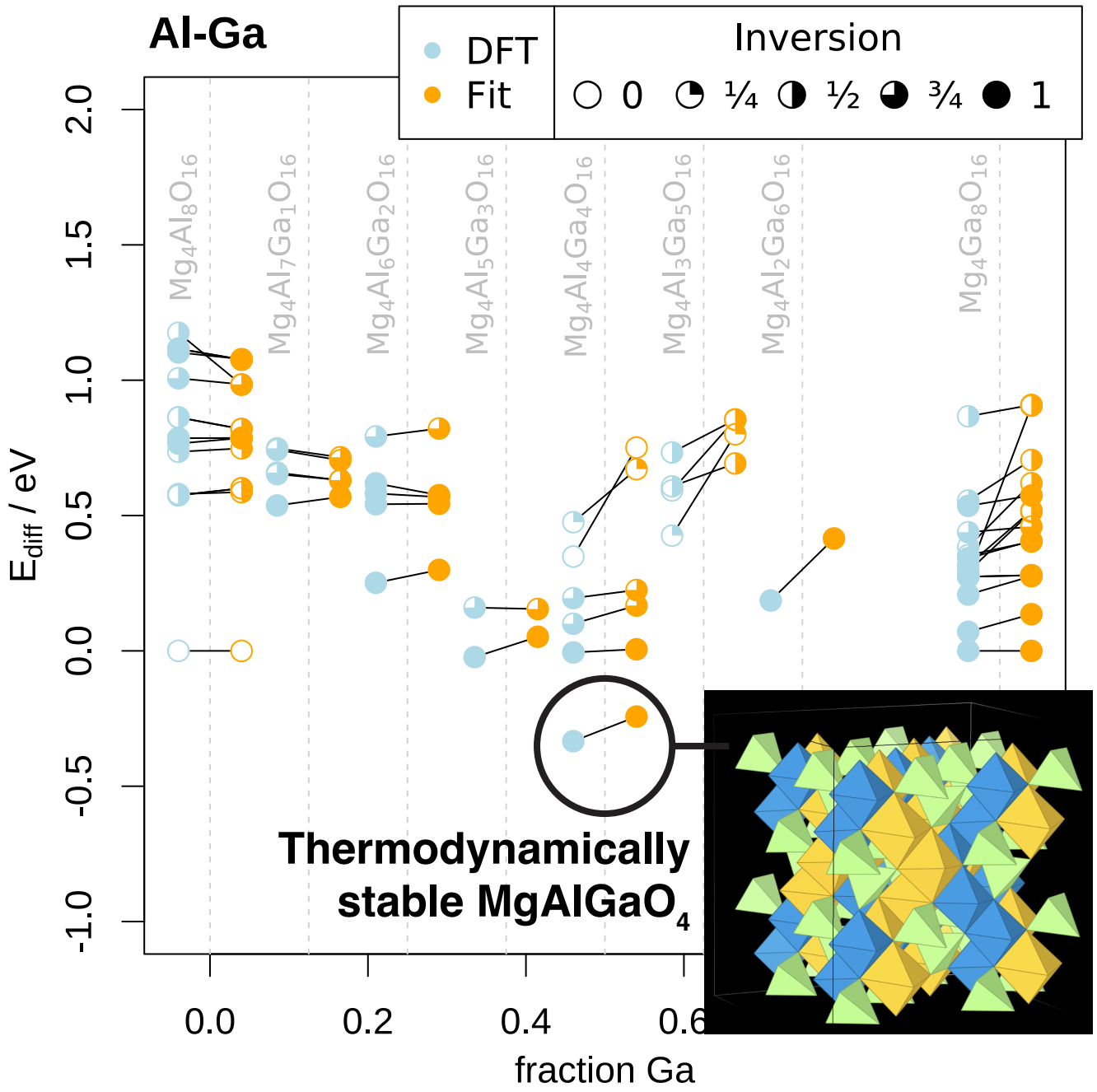

Highlights

A new interatomic potential for mixed Mg-Al-Ga-In spinels

Michael J. D. Rushton, Michael W. D. Cooper, Ghanshyam Pilania, Blas P. Uberuaga

- A new many-body potential for the mixed Mg-Al-Ga-In-O system has been derived, calibrated against energies from density functional theory.

- The new potential correctly predicts the thermodynamic stability of $MgAlGaO_4$ while also correctly predicting that $MgGaInO_4$ and $MgAlInO_4$ are unstable.

- The potential also provides a reasonable description of temperature-dependent elastic properties as compared to experiment.

A new interatomic potential for mixed Mg-Al-Ga-In spinels

Michael J. D. Rushton, Michael W. D. Cooper, Ghanshyam Pilania, Blas P. Uberuaga

[a]Nuclear Futures Institute, Bangor University, , Bangor, LL57 1UT, , United Kingdom
[b]Materials Science and Technology Division, Los Alamos National Laboratory, , Los Alamos, 87545, New Mexico, United States of America
[c]Materials Science and Technology Division, Los Alamos National Laboratory, , Los Alamos, 87545, New Mexico, United States of America
[d]GE Aerospace Research, , Niskayuna, 12309, New York, United States of America
[e]Materials Science and Technology Division, Los Alamos National Laboratory, , Los Alamos, 87545, New Mexico, United States of America

Abstract

While density functional theory (DFT) has become the de facto approach for accurate simulation of materials at the atomic scale, there are many aspects of materials that are simply out of reach of DFT methods. In particular, finite temperature properties such as diffusivities, the structure and properties of grain boundaries and interfaces, and the study of defect properties in complex alloys are computationally challenging for DFT methods. Recently, a new class of spinels in which three cations order over two sublattices was discovered. In order to predict the properties of these types of structures, classical potentials are a must. In this work, we derive a new classical potential for Mg-bearing spinels in which the B cations are Al, Ga, and/or In. The potential does well in describing the DFT energetics of various spinel structures as a function of chemistry and inversion. In particular, it reproduces the thermodynamically favorable $MgAlGaO_4$ structure while correctly predicting that neither $MgAlInO_4$ nor $MgGaInO_4$ are stable. Further, it reproduces physical trends in elastic properties as compared against experiment.

Keywords:
spinel, molecular dynamics, disorder, complex oxides

1. Introduction

Complex oxides, defined here as having more than one cation, offer tremendous potential in numerous technologies, from functional materials such as fast ion conductors and ferroelectrics to armor materials and even pigments. However, the same complexity that provides critical functionality also leads to challenges to understanding. A larger number of cations leads to more flexibility and variety of properties but also a greater structural and chemical space to examine to understand and design against. The typical approach of using density functional theory (DFT) to examine structure-property relationships for complex oxides is certainly very powerful, but becomes intractable as complexity grows. And while, from a simulation point of view, we will never replace DFT for the most accurate descriptions, it is extremely valuable to have classical potentials to examine scenarios that are currently, and for the foreseeable future, out of reach of DFT approaches.

A large range of phenomena require either longer simulation times or larger system sizes than can currently be treated with DFT alone. These include the structure and properties of grain boundaries, interfaces, and dislocations as well as the evolution of bulk and surface defects responsible for surface growth, radiation damage annealing, and sintering. While there are approaches such as the accelerated molecular dynamics methods [1] to extend the timescale of atomistic simulations, these are currently only efficient if using classical force fields. Even machine learned potentials [2, 3], while often reaching high levels of accuracy, are often too expensive for very long or very large simulations. Thus, for many practical systems of technological interest, we need classical models of interatomic interactions.

Spinels are a class of complex oxides that offer great promise for numerous functionalities. However, their chemical complexity requires classical models to complement DFT studies of their prop-

erties. In particular, a recently-discovered class of ordered 'double' spinels [4, 5] extends the space of spinel-structured materials but with additional chemical complexity. 'Single' spinels, with the generical chemical formula AB_2O_4 are known to exhibit various degrees of inversion - mixing between the cations on the tetrahedral site and the octahedral site - depending on chemistry, processing, temperature, and irradiation. Properties such as defect kinetics [6, 7, 8] and optical spectra [9] depend on the level of inversion. In the double spinels, with the formula $ABB'O_4$, three different cations can now mix and order across the two sublattices. This increases the chemical landscape of the material, further modifying defect properties.

An important aspect of these double spinels is that only some mixtures of single spinels will form a thermodynamically stable ordered double spinel [10, 4, 5]. For example, of the various possible combinations of mixing $MgAl_2O_4$ (hereafter referred to as MAO), $MgGa_2O_4$ (MGO), and $MgIn_2O_4$ (MIO), only the MAO+MGO mixture results in an ordered double spinel - $MgAlGaO_4$. To understand the thermokinetics associated with these more chemically complex materials, atomistic simulations of larger length and longer time than possible with DFT need to be performed, thus motivating the development of a new classical potential for these systems.

These mixed spinels offer new opportunities for functionality. For example, $MgGaAlO_4$ has been used as a catalyst for CO_2 [11]. Doped versions of the same compound have been studied for their luminescence properties [12] and as a near infrared long-afterglow material [13]. Solid solutions of $MgGaO_4$ and $MgInO_4$ have been considered for transparent conducitive oxides [14, 15, 16], as have mixtures of $MgAlO_4$ and $MgInO_4$ [17, 15]. Thus, there is a growing interest in understanding the properties of these materials and therefore a need to be able to describe their structure beyond the capabilities of DFT.

In this manuscript, we describe a new potential for MAO-MGO-MIO spinels that accurately describes the thermodynamic formation of the $MgAlGaO_4$ double spinel while at the same time predicting the instability of such a compound for MAO+MIO and MGO+MIO. We use the recently-derived CRG potential form [18], which allows us to describe subtle changes in coordination-dependent interactions in these compounds. With the new potential in hand, we then assess thermal properties that would be challenging if not outright impossible to consider with DFT methods. This new potential will allow for simulations of an exciting new spinel structure and provide new insight into the functionality of this new compound.

2. Methods

2.1. Definition of Inversion Level

Spinels are characterized by their level of inversion, or the degree to which the A and B cations mix across the two sublattices. In a normal AB_2O_4 spinel, with zero inversion, the A cations reside on the tehtrahedral sublattice while the B cations are on the octahedral sublattice. With increasing inversion, often denoted by the parameter i, there is greater mixing between the two sublattices. At full inversion $i = 1$, all of the tetrahedral sites are filled with B cations while the octahedral sublattice contains equal ratios of the two cations. Note that inversion is not the same as disorder. For a given level of inversion, the system can be fully ordered or exhibit some degree of disorder - the inversion parameter does not specify the disorder level. A fully random spinel, in which the cations are randomly distributed over the two sublattices, would have an inversion level $i = 2/3$.

2.2. Fitting Approach

An automated fitting approach was adopted for the development of the potential model. Potential fitting involves proposing an initial set of values to parametrise a potential model (described later, see X). The resulting model is then used to calculate structure and properties of a number atomic systems. These are then compared against a fitting database containing desired property values. By summing over the residual difference between the model candidates and database values, a figure of merit is defined. The intention of potential fitting is to minimise this merit value. In automated systems, such as that used here, optimisation algorithms iteratively adjust the potential parameters in order to gradually reduce the merit value so that property predictions of sufficient fidelity are obtained. In this work the initial stages of fitting used particle swarm optimisation [19] before switching to the Nelder Mead Simplex algorithm for final refinement of parameters [20, 21]. The implementation of the particle swarm algorithm provided in the Inspyred package was used [22],

whilst the simplex algorithm came from the Mystic package [23, 24]. The fitting procedure was coordinated by the Potential-Pro-Fit system created by Rushton [25].

The current potential model was fitted to a database of DFT values that were calculated in prior work [4]. This contained the 106 distinct spinel configurations that had been structurally relaxed using the VASP code. From these, relaxed atom positions, cell parameters, individual elastic constants (c_{11}, c_{12}, c_{13}, c_{33}, c_{44} and c_{66}) and energies were extracted, all of which were included in the fitting process. This was achieved by structural relaxation achieved via energy minimisation of each spinel configuration for the candidate classical potential model. The merit value was then obtained by summing the root mean squared differences between the properties obtained for the classical potential and the original DFT values. This sum was taken across all 106 spinel structures and chemistries. Energy minimisations were conducted using the GULP 5.0 [26, 27, 28] code which was controlled by our software for potential derivation [25].

During fitting to DFT energies, the enthalpy of mixing for each spinel structure was used. As it is also used in the results presented later, it is useful to show how this is calculated here. As discussed in Ref. [4], all energies were calculated using VASP [29, 30, 31, 32]. The mixing enthalpy of each double spinel configuration was computed relative to the energies of the ground state structures of each component single spinel:

$$\Delta E_{mix} = E_{MgBB'O_4} - \frac{1}{2}\left(E_{MgB_2O_4} + E_{MgB'_2O_4}\right) \quad (1)$$

2.3. Potential Model

The Finnis-Sinclair variation of the Embedded Atom Method (EAM) developed by Daw and Baskes was employed in this work [33]. Here it has been used to introduce a degree of environmental dependence to what is primarily a pair-potential model. The variation of inversion exhibited by the systems studied here gives rise to a wide range of distinct crystallographic environments. The aim of using the EAM, therefore, is to produce potential description that can adequately describe interactions for atoms in all these local configurations.

Equation 2 identifies the major components of the EAM model employed:

$$E_i = \frac{1}{2}\sum_j \phi_{\alpha\beta}(r_{ij}) - G_\alpha \sqrt{\sum_j \sigma_{\alpha\beta}(r_{ij})} \quad (2)$$

where E_i is the potential energy of an atom (i). The first sum calculates the pairwise interactions between i and surrounding atoms j. The distance between atom pairs (r_{ij}) is used to evaluate the pair contribution to the potential as the combination of an electrostatic and short-ranged component (the latter having a cut-off distance of 10 Å). These can be identified as the first and second terms in the following equation:

$$\phi_{\alpha\beta}(r_{ij}) = \left[\frac{q_\alpha q_\beta}{4\pi\epsilon_0 r_{ij}}\right] + \left[A_{\alpha\beta}\exp\left(\frac{-r_{ij}}{\rho_{\alpha\beta}}\right) - \frac{C_{\alpha\beta}}{r_{ij}^6}\right] \quad (3)$$

The charges on the interacting ions are q_i and q_j. In this work, partial charges have been used throughout with an ionicity of 2/3, meaning that the charge on oxygen was -1.33, whilst 2+ and 3+ cations had charges of 1.33 and 2.0, respectively. Long-range electrostatic interactions were calculated using the Ewald sum in GULP and the particle-particle particle-mesh solver in LAMMPS [34]. The ionicity, and hence the partial charges, were allowed to vary during the fit and good results were obtained for an ionicity of 2/3.

The second term in equation 3 describes short-ranged interactions and uses the Buckingham potential form [35]. The parameters $A_{\alpha\beta}$, $\rho_{\alpha\beta}$ and $C_{\alpha\beta}$ were adjusted during fitting to best describe the interaction betwen species pairs $\alpha\beta$.

We now move our attention to the many bodied component of the model ($-G_\alpha\sqrt{\sum_j \sigma_{\alpha\beta}(r_{ij})}$ in equation 2). Here $\sigma_{\alpha\beta}$ is known as the density function and the sum is over this notional electronic density for the atoms surrounding the central atom, i. The density sum is then passed through an embedding function (here, negative square root) to yield the many body term. G_α, the embedding parameter, is another fitting parameter and this adjusts the scale of the electronic density embedded around atom i of species α. The form of the density function is now given:

$$\sigma_{\alpha\beta}(r_{ij}) = \frac{n_{\alpha\beta}}{r_{ij}^{12}} \quad (4)$$

The $n_{\alpha\beta}$ parameter is the last adjustable parameter included in the fitting procedure. As noted

Pair interaction ($\alpha - \beta$)	$A_{\alpha\beta}$ (eV)	$\rho_{\alpha\beta}$ (Å)	$C_{\alpha\beta}$ (eVÅ^6)
O-O	7796.75403	0.259721	0.0
Mg-O	3532.24990	0.226573	0.746495
Al-O	15002.73002	0.196772	37.817297
Ga-O	4005.37109	0.234466	8.8441193
In-O	3627.22434	0.249864	0.0

Table 1: Parameters for pairwise component of the potential model. All parameters not explicitly provided were set to zero. In particular, there is no pairwise interactions between cations beyond the Coulomb interaction.

Interaction ($\alpha - \beta$)	$n_{\alpha\beta}$
Ga-O	23942.18
In-O	70000.00

Table 2: Density function parameter for the embedded atom model component of the potential model. All parameters not explicitly provided were set to zero.

Species (α)	G_α (eVÅ$^{1.5}$)
Ga	0.14502465
In	0.01069124

Table 3: Embedding function parameter for the embedded atom model component of the potential model. All parameters not explicitly provided were set to zero.

above, the Finnis-Sinclair variant of the embedded atom method has been used. In the original EAM the same function is used to calculate the density of a particular species. In the Finnis-Sinclair version, however, density functions are specified for each pair of species. This means that a different value of $n_{\alpha\beta}$ may be used to calculate the oxygen density embedded around a gallium atom ($n_{\text{Ga-O}}$) than for the oxygen density around indium ($n_{\text{In-O}}$). This has been used here so that only the oxygen density is calculated around Ga and In.

3. Results

In this section the results of the fitting procedure will be reported. The model is then validated by comparing property values calculated using the fitted model with available experimental data. Finally, model predictions are given and described to help increase understanding of these spinel systems.

The potential model parameters resulting from the fitting process are given in Tables 1, 2 and 3. The pair parameters for equation 3 are given in Table 1. For the many-body interactions, the value of the embedding parameter, G_α from equation 2 appear in Table 3 whilst the values for the density function (equation 4) are given in Table 2. Plots of the different functions are provided in Fig. 1, which highlights that all of the functions are smooth with no spurious cusps or sharp derivatives.

3.1. Quality of Fit

Figures 2–4 compare the enthalpies of formation from the DFT fitting database with those predicted by the classical potential model derived for this work. The three compositional axes (Al-Ga, Ga-In and Al-In) are plotted in Figures 2, 3 and 4, respectively. In these, the expected (DFT) and fitted energies are plotted as pairs, linked by lines to give the appearance of a dumbbell. Each DFT energy (blue) its connected to its classical counterpart (orange) by a line centered above a particular composition on the x-axis. As described earlier, the DFT fitting database contained multiple structures for each spinel composition, with the degree of inversion sometimes varying even for the same composition. This is shown in the figures by the degree of infill each point has. An empty point has the normal spinel structure whilst a filled point is fully inverted; the $\frac{1}{4}$, $\frac{1}{2}$ and $\frac{3}{4}$ fill fractions showing those intermediate levels of inversion.

Another way to show the quality of the obtained fit against the reference DFT is to use a parity plot of the type shown in Figure 5. This plots the expected DFT enthalply of mixing against those obtained from the potential. Parity is represented by a line with a slope of one passing through the origin (shown in the figure as a dashed black line). As would be expected the majority of points are clustered close to this line. It should be noted that points at the upper end of both the DFT and potential axes represent structures with high enthalpies of mixing. These are unlikely to form when compared to those in the bottom left corner of the plot. An important property of the potential model is that it correctly predicts the correct low energy structure for each spinel composition. The effect of this can be seen in the parity plot (Figure 5) by the close correspondence between the dashed line and structures with formation energies less than 0.5 eV, in the lower left quarter of the figure.

Returning to the dumbbell plots for a moment

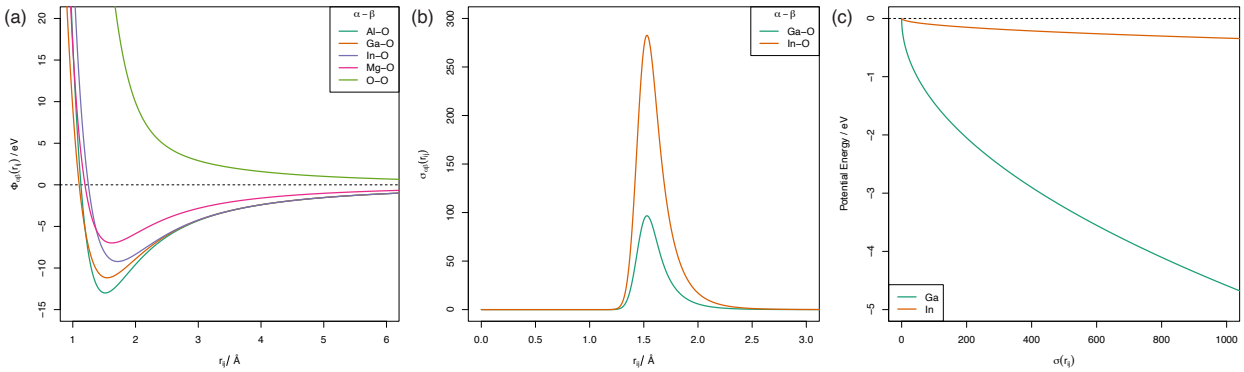

Figure 1: Plots of the various functions defining the potential. (a) The pairwise functions versus atom separation. (b) The density function versus atom separation. (c) The energy versus the density function.

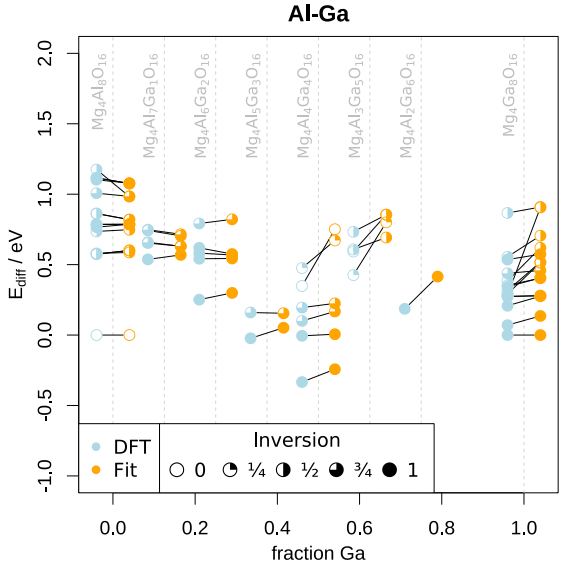

Figure 2: Comparison of derived potential model with DFT energies for the Al-Ga system. The RMSE for the potential for this system is 0.146 eV.

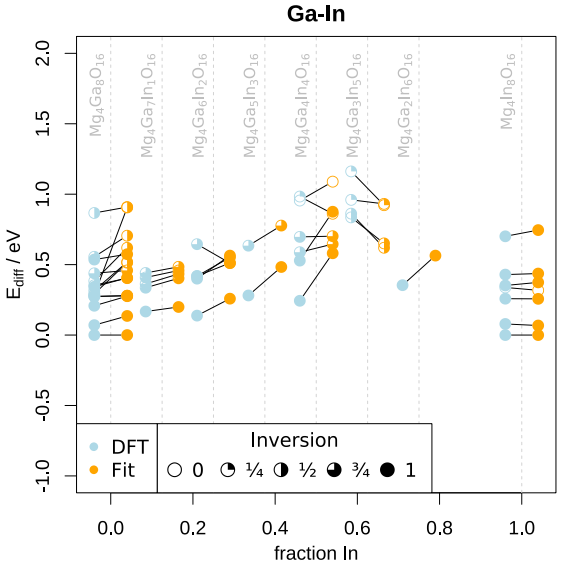

Figure 3: Comparison of derived potential model with DFT energies for the Ga-In system. The RMSE for the potential for this system is 0.168 eV.

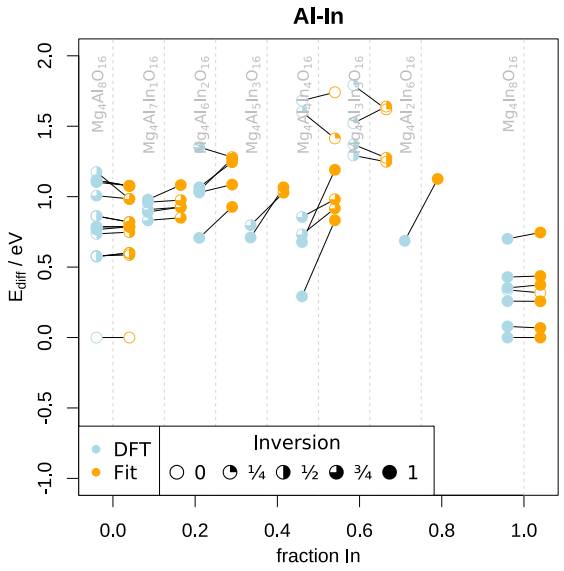

Figure 4: Comparison of derived potential model with DFT energies for the Al-In system. The RMSE for the potential for this system is 0.164 eV.

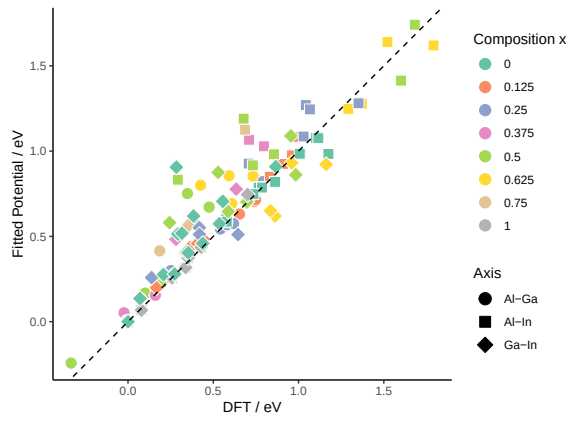

Figure 5: Parity plot comparing the formation energies obtained from DFT with the fitted potential model. Points falling on the dashed line have the same energy in both DFT and potential model calculations.

(Figures 2–4), if the classical potential model had been able to perfectly replicate the DFT energies then the dumbbells for each energy pair would all be horizontal, showing an energy difference between the classical and DFT values of 0 eV. Although a great many structures are close to this ideal, there are also some with significant energy differences (steep lines). Similarly, these plots provide a rapid visual check as to whether the potential model energies occur in the same sequence as DFT. When they do not, crossed lines are apparent. In general, the potential model has done well in preserving the correct ordering, particularly when the more thermodynamically stable structures, at lower formation energies, are considered. Again it should be emphasised that in all cases the lowest energy structure for each composition is the same for both DFT and potential models. This also means that the model also reproduces the important result by Pilania et al. that a negative enthalpy of mixing can be obtained for an equimolar $MgAl_2O_4$-$MgGa_2O_4$ composition (i.e. the lowest energy structure in Figure 2 with fraction Ga = 0.5) [4].

3.2. *Thermomechanical Properties*

Bulk moduli were calculated as a function of temperature for the new potential model. Properties were obtained for the lowest energy structures for each spinel composition (see Figures 2–4) using the following process. Bulk modulus (k) measures a material's elastic response to changes in volume:

$$k = -V\frac{dP}{dV}$$

where P is pressure and V is volume. A series of molecular dynamics runs, performed using the LAMMPS simulation package [34], was conducted in order to establish the relaxed volume and pressure derivative at a given temperature. The temperature of the system was initialised through 5 ps of MD in the NPT ensemble (allowing cell lengths to relax to zero pressure) using a Nosé-Hoover thermostat and barostat using relaxation parameters of 0.04 ps and 0.1 ps respectively [36, 37, 38]. The relaxed volume was obtained through a further 10 ps of NPT dynamics, the volume being averaged over the final 8 ps.

To allow a numerical derivative to be taken, five simulations boxes were created based on this relaxed volume, each containing 1792 atoms, the vol-

umes of which were scaled to be above and below the relaxed volume established in the previous step. The cell lengths for these boxes used scaling factors of 0.98, 0.99, 1.00, 1.01 and 1.02 respectively. These were then equilibrated in the NVT ensemble (holding their cell lengths fixed) with 2 ps of dynamics to establish the target temperature and a further 8 ps during which the average pressure of the system was taken. Temperature was again controlled using a Nosé-Hoover thermostat. The $\frac{dP}{dV}$ derivative was then established, for the relaxed unstrained box volume, via a quadratic fit to the pressure vs volume data obtained from scaled simulation boxes. In this way, bulk moduli were obtained for temperatures between 300K and 2000K in steps of 50K.

It is useful to compare the bulk moduli produced by the potential model with comparable experimental measurements. The majority of the mixed double spinels used to derive the potential model had positive mixing enthalpies [4]. This means that many of them are unlikely to form and whilst efforts are underway to synthesise the composition which shows a negative mixing enthalpy, experimental property data for the double spinel systems is currently unavailable. Despite this, values for the single spinel end-members are more readily available. Figure 6 plots MD derived bulk moduli alongside experimental measurements made by Askarpour et al. for $MgAl_2O_4$ [39]. A similar comparison is made for $MgGa_2O_4$ in Figure 7 using the experimental data of Hirschle et al. [40]. Experimental bulk modulus measurements could not be found for the $MgIn_2O_4$ end-member.

The MD results provide a good match to the experimental trend in bulk modulus with temperature for $MgAl_2O_4$ as shown in Figure 6. The experimental data shows a linear downward trend as temperature increases. Whilst there is a good deal of overlap between both MD and the Askarpour data [39], this trend is slightly steeper for the simulation data, meaning it over-predicts bulk modulus below 500 K and underpredicts over 1000 K. Also included in Figure 6 is a dashed horizontal line showing the bulk modulus value obtained from static DFT calculations. This is effectively a value taken at T=0K and shows that the DFT tends to underpredict the bulk modulus for this material.

The results for $MgGa_2O_4$ (Figure 7) again show that DFT tends to underpredict the experimental values of Hirschle et al. [40]. In this case, however,

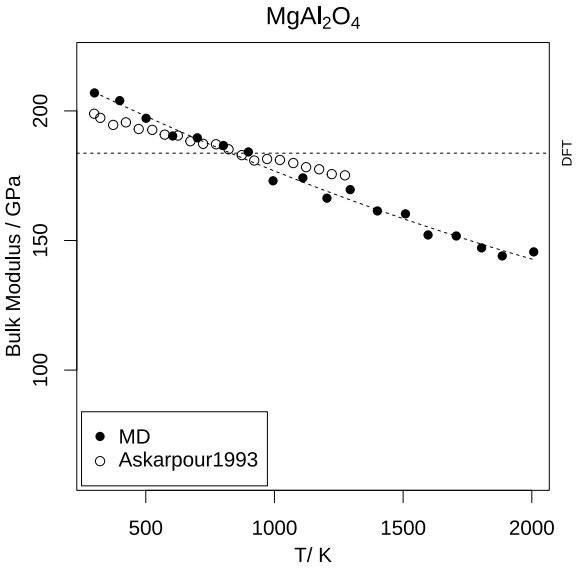

Figure 6: Bulk modulus as a function of temperature for spinel end-member $MgAl_2O_4$. Molecular dynamics (MD) data are compared with experimental values from Askarpour et al. (open symbols) [39]. Horizontal dashed line indicates bulk-modulus obtained from static DFT calculations.

}

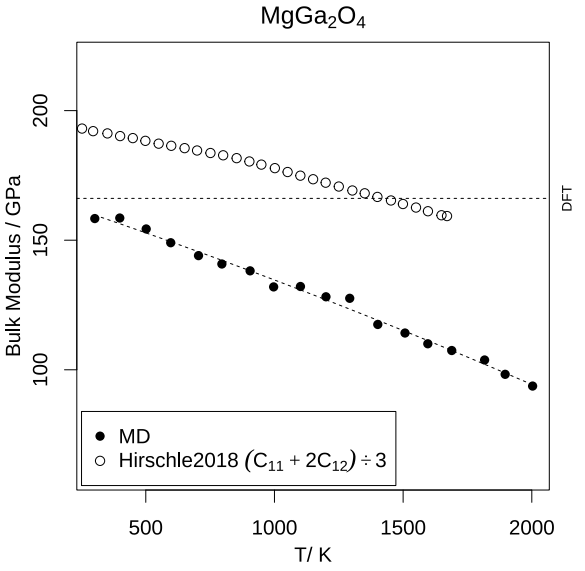

Figure 7: Bulk modulus as a function of temperature for spinel end-member $MgGa_2O_4$. Molecular dynamics (MD) data are compared with experimental values where possible (open symbols). Horizontal dashed line indicates bulk-modulus obtained from static DFT calculations.

the classical potential produces bulk moduli that are always lower than both DFT and experiment within the plotted temperature range (300–2000K). The difference between the MD and experimental data is 34 GPa at 300K and 51 GPa at 1600K.

Bulk moduli are shown visually as heatmaps in Figure 8. These plot temperature along the vertical axis and composition along the horizontal axis, with the colour of each cell showing the bulk modulus. Hot colours indicate high values while cool colours indicate lower values of the modulus. Three maps are provided, one for each of the double spinel compositional ranges (Al-Ga, Al-In and Ga-In). Each vertical bar in these maps represents the lowest energy structure for a given composition and shows the bulk modulus as temperature increases on moving up the plot. Additionally, the degree of inversion is given for each low energy structure's respective bar.

All the systems show bulk modulus decreasing with temperature. The Al-Ga spinels tended to be slightly stiffer than the other systems with a maximum modulus of 219 GPa (x=0.125 at T=300K) which decreases to a minimum of 91 GPa (x=0.625 at T=2000K). By comparison, the ranges for the Al-In and Ga-In systems were 69–207 GPa and 69–158 GPa respectively. For these two cases, both minimum values occurred for x=1.0 and T=2000K whilst they were highest at x=0.0 and T=300K.

In general, the gradations in colour across the heat maps are relatively smooth, indicating progressive changes in bulk modulus as composition and temperature vary. Despite this general trend, when moving along the composition axes there are some points which show more abrupt changes. For instance, in the Al-Ga heatmap there is a step up in modulus between x=0 and x=0.125, when the trend in the surrounding data is for it to decrease. There is a similar step down between x=0.5 and x=0.625 before a slight increase to x=0.75. These slight jumps can be shown more clearly by plotting the bulk moduli as a function of composition for a single temperature. This is shown for T=300 K in Figure 9 for all three double spinel compositional ranges. Each point in this figure has also been labelled with its corresponding structure's degree of inversion. These help show that abrupt changes in the trend in bulk modulus with x occur when the degree of inversion changes in relation to surrounding points. The abrupt changes noted for the Al-Ga structures above are consistent with this. The increase in modulus between x=0.0

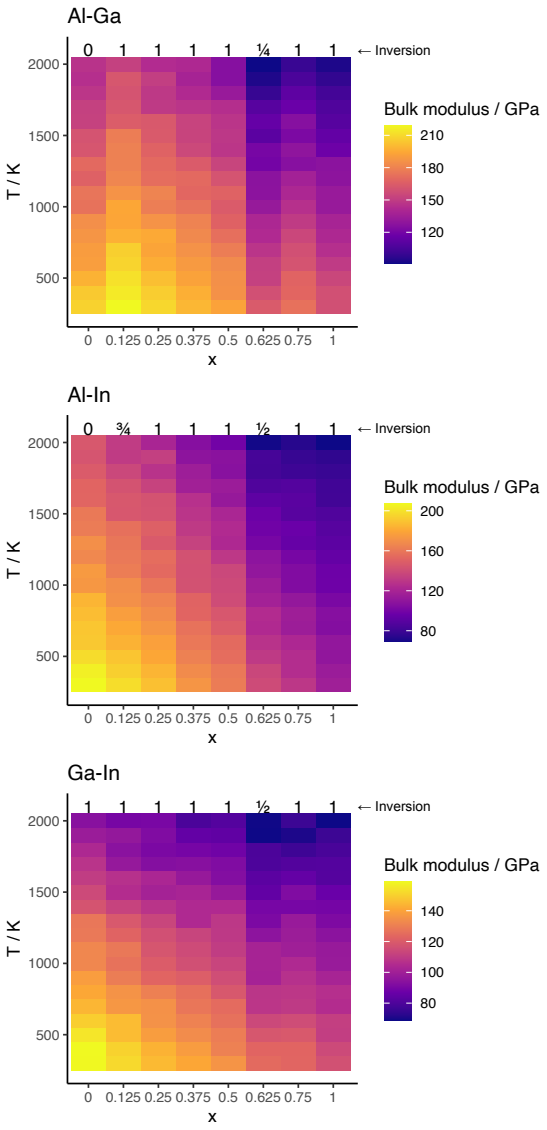

Figure 8: Heatmap showing bulk moduli values for the low energy systems calculated from potential model using molecular dynamics.

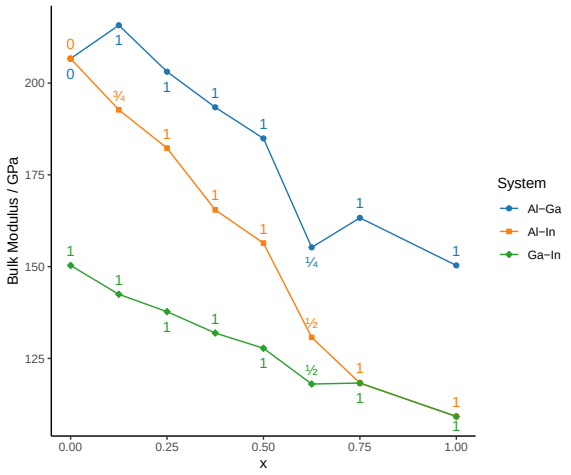

Figure 9: Bulk modulus as a function of composition (x) at T=300 K for the lowest energy structures from the three spinel systems. The numbers above and below each point show the degree of inversion for that structure.

and x=0.125 coincides with the inversion changing from 0 to 1. Similarly the dip in bulk modulus at x=0.625 happens when the inversion goes from 1 to $\frac{1}{4}$ and back again. A similar but smaller changes is observed for Ga-In at x=0.625 with inversion changing from 1 to $\frac{1}{2}$. Inversion has less of an effect in the Al-In plot, with the difference in bulk modulus at the points where inversion changes (at x=0.125 and x=0) being similar to where inversion remains the same.

4. Discussion and Conclusions

Overall, the new potential does a reasonable job in describing the properties of mixed Al-Ga, Al-In, and Ga-In spinels. In particular, the relative energetics of different compositions for each series and different levels of inversion for a given composition agree well with the DFT dataset. Certainly there are discrepancies, but these tend to occur for higher energy structures that are less thermodynamically relevant. Most critically, the potential correctly describes the negative heat of mixing for the Al-Ga system at the 50/50 composition, suggesting it would be suitable for studying the properties of the $MgAlGaO_4$ double spinel structure.

The new potential represents a significant improvement in the description of the mixed spinels as compared to the literature potential of Bacorisen et al. [41]. While that potential does predict a thermodynamically stable $MgAlGaO_4$ structure, it is different than the one predicted by DFT. Further, the one predicted by DFT is predicted to be much higher in energy and thermodynamically unstable with the Bacorisen potential. Finally the RMSE for that potential for all of the structures considered in Fig. 2 is much higher with that potential than the new one described here: 0.64 eV vs 0.14 eV. Thus, while that potential has been successful in modeling the individual spinels [41, 42, 6, 43], it is less suitable for these mixed compounds.

The new potential also does well for elastic properties at ambient conditions as compared to prior experiment and DFT. Temperature-dependent comparisons of the bulk modulus are provided in Figs. 6–7. Further studies have found values of the bulk modulus of 197.9±0.2(experiment) [44] and 208 GPa (DFT) [45] for $MgAl_2O_4$, 163 GPa (DFT) [45] for $MgGa_2O_4$ and 132 GPa (DFT) [45] for $MgIn_2O_4$. As shown in Figs. 6–7, our potential agrees well with these values (for reference, our potential finds a bulk modulus for $MgIn_2O_4$ of 116.44 GPa). Note that these two studies emphasize the behavior of elastic constants under pressure, something which we have not considered here.

The temperature dependent bulk moduli are also reasonably described as compared to experiment for the cases where experimental data exists. Importantly, trends with temperatures are well reproduced even if the absolute magnitude for $MgGa_2O_4$ is less well described. This gives some confidence that finite temperature properties will be reasonably well described by the new potential.

As with all classical potentials, not all properties are perfectly reproduced. We hope and expect that physical trends with changes in chemisty are well described by the potential and that is what our analysis shows. We thus expect that this new potential will be valuable for atomistic studies of more complex spinel chemistries involving multiple B cations.

Further, given the classical nature of this potential, there are inherent limitations to the physics it can describe. Chief amongst those are charge transfer processes. While the cations in these three spinels exhibit relatively little variation in valence state, the potential cannot describe any variation in charge state. Thus, for example, this potential cannot describe charged defects. In addition, the potential has not been tested for behavior under pressure and thus may not be suitable for high pres-

sure simulations. Finally, we have not assessed the vibrational entropy of higher temperature structures, which is important for understanding the high temperature stability of these compounds. Thus, while the potential reproduces the 0 K stability of these compounds as predicted by DFT, we have not determined how stable these compounds would be at higher temperature.

To conclude, we have developed a new interatomic potential for Mg-based spinels containing Al, Ga, and/or In. The potential reproduces the DFT-predicted stability of mixed Al-Ga spinel and the instability of Al-In and Ga-In spinels. Temperature-dependent properties are also reasonably reproduced. This new potential should open new opportunities for understanding the properties of more complex spinel chemistries and provide insight into new possible functionalities.

5. Acknowledgements

This work was supported by the U.S. Department of Energy, Office of Science, Basic Energy Sciences, Materials Sciences and Engineering Division. This research used resources provided by the Los Alamos National Laboratory Institutional Computing Program, which is supported by the U.S. Department of Energy National Nuclear Security Administration under Contract No. 89233218CNA000001. Los Alamos National Laboratory is operated by Triad National Security, LLC, for the National Nuclear Security Administration of U.S. Department of Energy (Contract No. 89233218CNA000001).

6. Data Availability

The potential files, including a README with details on using the potential, are included in the Supplemental Information. The rest of the data that support the findings of this article are not publicly available. The data are available from the authors upon reasonable request.

References

[1] Danny Perez, Blas P Uberuaga, Yunsic Shim, Jacques G Amar, and Arthur F Voter. Accelerated molecular dynamics methods: introduction and recent developments. *Annual Reports in computational chemistry*, 5:79–98, 2009.

[2] Volker L Deringer, Miguel A Caro, and Gábor Csányi. Machine learning interatomic potentials as emerging tools for materials science. *Advanced Materials*, 31(46):1902765, 2019.

[3] Ryan Jacobs, Dane Morgan, Siamak Attarian, Jun Meng, Chen Shen, Zhenghao Wu, Clare Yijia Xie, Julia H Yang, Nongnuch Artrith, Ben Blaiszik, et al. A practical guide to machine learning interatomic potentials–status and future. *Current Opinion in Solid State and Materials Science*, 35:101214, 2025.

[4] Ghanshyam Pilania, Vancho Kocevski, James A. Valdez, Cortney R. Kreller, and Blas P. Uberuaga. Prediction of structure and cation ordering in an ordered normal-inverse double spinel. *Communications Materials*, 1(1):84, November 2020.

[5] Vancho Kocevski, Ghanshyam Pilania, and Blas P Uberuaga. High-throughput investigation of the formation of double spinels. *Journal of Materials Chemistry A*, 8(48):25756–25767, 2020.

[6] Blas P Uberuaga, D Bacorisen, Roger Smith, JA Ball, RW Grimes, Arthur Ford Voter, and KE Sickafus. Defect kinetics in spinels: Long-time simulations of mg al 2 o 4, mg ga 2 o 4, and mg in 2 o 4. *Physical Review B—Condensed Matter and Materials Physics*, 75(10):104116, 2007.

[7] Blas P Uberuaga and Ghanshyam Pilania. Inversion, chemical complexity, and interstitial transport in spinels. *Journal of the American Ceramic Society*, 104(5):2313–2324, 2021.

[8] Peter Hatton and Blas Pedro Uberuaga. Short range order in disordered spinels and the impact on cation vacancy transport. *Journal of Materials Chemistry A*, 11(7):3471–3480, 2023.

[9] Luis I Granone, Anna C Ulpe, Lars Robben, Stephen Klimke, Moritz Jahns, Franz Renz, Thorsten M Gesing, Thomas Bredow, Ralf Dillert, and Detlef W Bahnemann. Effect of the degree of inversion on optical properties of spinel znfe 2 o 4. *Physical Chemistry Chemical Physics*, 20(44):28267–28278, 2018.

[10] ZhiBin Chen, Honglin Tan, Lan Yu, and Chao Xiang. Ab initio study of the opto-electronic and elastic properties of mgga x al (2- x) o 4. *The European Physical Journal B*, 88:1–8, 2015.

[11] Xiaoyu Zhang, Wenqiang Liu, Peng Peng, Zhijie Zhang, Qinglin Du, Jiayu Shi, and Lidan Deng. A dual functional sorbent/catalyst material for in-situ co2 capture and conversion to ethylene production. *Fuel*, 351:128701, 2023.

[12] ND Tran, EF Polisadova, and VM Lisitsyn. Structure and properties of mgal2o4: Eu3+ and mgalgao4: Eu3+ spinel ceramics produced by radiation synthesis. *Russian Physics Journal*, 67(5):632–641, 2024.

[13] Keliang Qiu, Panlai Li, Xiangyu Meng, Jinjin Liu, Qi Bao, Yuebin Li, Xue Li, Zhipeng Wang, Zhiping Yang, and Zhijun Wang. Trap distribution and mechanism for near infrared long-afterglow material almggao 4: Cr 3+. *Dalton Transactions*, 48(2):618–627, 2019.

[14] Toshihiro Moriga, Takashi Sakamoto, Yoshiki Sato, Azrul Hisham Khalid, Ryoichi Suenari, Ichiro Nakabayashi, et al. Crystal structures and electrical and optical properties of mgin2- xgaxo4solid solutions. *Journal of Solid State Chemistry*, 142(1):206–213, 1999.

[15] Altynbek Murat and Julia E Medvedeva. Electronic properties of layered multicomponent wide-band-gap oxides: A combinatorial approach. *Physical Review B—Condensed Matter and Materials Physics*, 85(15):155101, 2012.

[16] Takehiro Koike, Hena Das, Kengo Oka, Yoshihiro Kusano,

Fernando Cubillas, Francisco Brown Bojorqez, Victor Emmanuel Alvarez-Montano, Shigekazu Ito, Kei Shigematsu, Hayato Togano, et al. Pressure-induced ybfe2o4-type to spinel structural change of ingamgo4. *Solids*, 5(3):422–433, 2024.

[17] Julia E Medvedeva. Averaging of the electron effective mass in multicomponent transparent conducting oxides. *Europhysics Letters*, 78(5):57004, 2007.

[18] MWD Cooper, MJD Rushton, and RW Grimes. A many-body potential approach to modelling the thermomechanical properties of actinide oxides. *Journal of Physics: Condensed Matter*, 26(10):105401, 2014.

[19] Kalyanmoy Deb and Nikhil Padhye. Development of efficient particle swarm optimizers by using concepts from evolutionary algorithms. In *Proceedings of the 12th annual conference on Genetic and evolutionary computation*, pages 55–62, Portland Oregon USA, July 2010. ACM.

[20] J. A. Nelder and R. Mead. A Simplex Method for Function Minimization. *The Computer Journal*, 7(4):308–313, January 1965.

[21] J. A. Nelder and R. Mead. Errata: A simplex method for function minimization. *The Computer Journal*, 8(1):27–27, April 1965.

[22] Alberto Tonda. Inspyred: Bio-inspired algorithms in Python. *Genetic Programming and Evolvable Machines*, 21(1-2):269–272, June 2020.

[23] Michael M. McKerns, Leif Strand, Tim Sullivan, Alta Fang, and Michael A. G. Aivazis. Building a Framework for Predictive Science, 2012. Version Number: 1.

[24] Michael M. McKerns, Patrick Hung, and Michael A. G. Aivazis. mystic: highly-constrained non-convex optimization and UQ, 2009.

[25] M.J.D. Rushton. Potential Pro-Fit, June 2023.

[26] J.D Gale. General Utility Lattice Program Version 5.0.

[27] J. D. Gale. GULP - a computer program for the symmetry adapted simulation of solids. *Journal of the Chemical Society Faraday Transactions*, 93(4):629–637, 1997.

[28] J. D. Gale and A. L. Rohl. The General Utility Lattice Program (GULP). *Molecular Simulation*, 29(5):291–341, May 2003.

[29] G. Kresse and J. Hafner. Ab initiomolecular dynamics for liquid metals. *Physical Review B*, 47(1):558–561, jan 1993.

[30] G. Kresse and J. Hafner. Ab initiomolecular-dynamics simulation of the liquid-metal–amorphous-semiconductor transition in germanium. *Physical Review B*, 49(20):14251–14269, may 1994.

[31] G. Kresse and J. Furthmüller. Efficiency of ab-initio total energy calculations for metals and semiconductors using a plane-wave basis set. *Computational Materials Science*, 6(1):15–50, jul 1996.

[32] G. Kresse and J. Furthmüller. Efficient iterative schemes forab initiototal-energy calculations using a plane-wave basis set. *Physical Review B*, 54(16):11169–11186, oct 1996.

[33] Murray S Daw and Michael I Baskes. Embedded-atom method: Derivation and application to impurities, surfaces, and other defects in metals. *Physical Review B*, 29(12):6443, 1984.

[34] A. P. Thompson, H. M. Aktulga, R. Berger, D. S. Bolintineanu, W. M. Brown, P. S. Crozier, P. J. in 't Veld, A. Kohlmeyer, S. G. Moore, T. D. Nguyen, R. Shan, M. J. Stevens, J. Tranchida, C. Trott, and S. J. Plimpton. LAMMPS - a flexible simulation tool for particle-based materials modeling at the atomic, meso, and continuum scales. *Comp. Phys. Comm.*, 271:108171, 2022.

[35] R. A. Buckingham. The Classical Equation of State of Gaseous Helium, Neon and Argon. *Proceedings of the Royal Society of London. Series A, Mathematical and Physical Sciences (1934-1990)*, 168(933):264–283, October 1938. Publisher: Printed for the Royal Society and sold by Harrison Sons Place: London.

[36] S. Nosé. A Unified Formulation of the Constant Temperature Molecular Dynamics Methods. *The Journal of Chemical Physics*, 81(1):511, 1984. Publisher: American Institute of Physics Place: [Woodbury, N.Y.].

[37] S. Nosé. A molecular dynamics method for simulations in the canonical ensemble. *Molecular Physics*, 52(2):255–268, June 1984.

[38] William G Hoover. Canonical Dynamics: Equilibrium Phase-space Distributions. *Physical review.B, Condensed matter*, 31(3):1695, March 1985. Publisher: Published for the American Physical Society by the American Institute of Physics Place: New York, N.Y.

[39] V. Askarpour, M. H. Manghnani, S. Fassbender, and A. Yoneda. Elasticity of single-crystal MgAl2O4 spinel up to 1273 K by Brillouin spectroscopy. *Physics and Chemistry of Minerals*, 19(8):511–519, 1993.

[40] C. Hirschle, J. Schreuer, and Z. Galazka. Interplay of cation ordering and thermoelastic properties of spinel structure MgGa2O4. *Journal of Applied Physics*, 124(6), 2018.

[41] Dnyansingh Bacorisen, Roger Smith, JA Ball, RW Grimes, Blas P Uberuaga, KE Sickafus, and WT Rankin. Molecular dynamics modelling of radiation damage in normal, partly inverse and inverse spinels. *Nuclear instruments and methods in physics research section B: Beam interactions with materials and atoms*, 250(1-2):36–45, 2006.

[42] D Bacorisen, Roger Smith, Blas P Uberuaga, KE Sickafus, JA Ball, and RW Grimes. Atomistic simulations of radiation-induced defect formation in spinels: Mg al 2 o 4, mg ga 2 o 4, and mg in 2 o 4. *Physical Review B—Condensed Matter and Materials Physics*, 74(21):214105, 2006.

[43] M Saraiva, Violeta Georgieva, Stijn Mahieu, Koen Van Aeken, Annemie Bogaerts, and Diederik Depla. Compositional effects on the growth of mg (m) o films. *Journal of Applied Physics*, 107(3), 2010.

[44] Akira Yoneda. Pressure derivatives of elastic constants of single crystal mgo and mgal2o4. *Journal of Physics of the Earth*, 38(1):19–55, 1990.

[45] A Bouhemadou, R Khenata, and FJTEPJB Zerarga. Ab initio study of the structural and elastic properties of spinels mgx2o4 (x= al, ga, in) under pressure. *The European Physical Journal B*, 56(1):1–5, 2007.